Low Temperature Physics/Fizika Nizkikh Temperatur, 2012, v. 38, No. 9, pp. 1032–1040

Spin dynamics of S = 1/2 Heisenberg chains with a staggered transverse field: electron spin resonance studies

(Review Article)

S.A. Zvyagin

Dresden High Magnetic Field Laboratory (HLD), Helmholtz-Zentrum Dresden-Rossendorf, 01328 Dresden, Germany

E-mail: s.zvyagin@hzdr.de

Received April 18, 2012

In this article I review recent achievements on experimental studies of magnetic excitations in the copper pyrimidine dinitrate $[PM–Cu(NO_3)_2(H_2O)_2]_n$ (PM = pyrimidine), an S = 1/2 antiferromagnetic chain material with alternating g-tensor and the Dzyaloshinskii–Moriya interaction, by means of high-field electron spin resonance (ESR). Due to this alternation, in the 1D critical regime this material exhibits a field-induced gap. The excitation spectrum is formed by solitons and their bound states, breathers, and can be effectively described using the sine-Gordon model. With increasing temperature, the soliton-breather regime can be suppressed, resulting in a substantial evolution of ESR parameters. These changes can be described using a new theoretical concept recently proposed for $S = 1/2$ AF chains with a staggered transverse field. High magnetic field induces a transition into spin-polarized state with the excitation spectrum formed by magnons. Nonmonotonous behavior of the field-induced gap is observed in the vicinity of saturation field. The experimental data are compared with results of existing theoretical approaches, revealing an excellent agreement with the predictions.

PACS: 75.40.Gb Dynamic properties (dynamic susceptibility, spin waves, spin diffusion, dynamic scaling, etc.);
76.30.–v Electron paramagnetic resonance and relaxation;
75.10.Jm Quantized spin models, including quantum spin frustration.

Keywords: antiferromagnetic chain, electron spin resonance, Dzyaloshinskii–Moriya interaction, high magnetic field.

Contents

1. Introduction

Recently, a considerable amount of attention has been given to theoretical and experimental investigations of low-dimensional (hereafter low-D) spin systems. Among others, 1D Heisenberg antiferromagnetic (AF) chain is one of the paradigm models of quantum magnetism. The ground state of an isotropic $S = 1/2$ Heisenberg AF chain with uniform nearest-neighbor exchange coupling is a spin singlet, and its dynamics is determined by a gapless two-particle continuum of $S = 1/2$ excitations, known as spinons. A uniform magnetic field causes a substantial rearrangement of the excitation spectrum, making the soft modes incommensurate [1,2] but leaving the spinon continuum gapless. Since the $S = 1/2$ AF chain is critical, even small perturbations can considerably change ground-state properties of the system. One of the most fundamental and interesting examples to that respect is the $S = 1/2$

AF chain perturbed by an alternating *g*-tensor or the Dzyaloshinskii–Moriya (DM) interaction. As shown recently, in the presence of such alternation, application of a uniform field H induces an effective transverse staggered field, $h \propto H$, which leads to the opening of an energy gap, $\Delta \propto H^{2/3}$ [3]. This situation is realized experimentally in a number of spin chain materials, for instance, copper benzoate $Cu(C_6H_5COO)_2{\cdot}3H_2O$ [4], copper pyrimidine dinitrate [5], Yb_4As_3 [6], $CuCl_2$ (dimethylsulfoxide) [7], and $KCuGaF_6$ [8]. The excitation spectrum of such a system can be effectively described employing the sine-Gordon quantum field theoretical approach [3,9]. In accordance with that theory, the spin dynamics in the 1D critical regime (when the temperature T is small compared to the energy gap Δ) is represented by solitons, antisolitons, and multiple soliton–antisoliton bound states, or breathers. Importantly, the availability of exact solutions for the sine-Gordon model allows very accurate description of many observable properties and physical parameters of $S = 1/2$ AF chain systems perturbed by an alternating *g*-tensor or the DM interaction, including field dependence of excitation energies [3,9,10] and response functions [11,12].

Electron spin resonance (ESR) has proven to be a very powerful method to probe spin dynamics in solids [13]. Compared to many other spectroscopy techniques, ESR has several distinct and important advantages. First, it allows to measure very small (of mm- and submm-size scale) samples. Second, ESR is known for its outstanding spectral resolution and sensitivity. Third, based on the recent progress in the high-field technologies, ESR becomes more and more popular tool to probe magnetic excitations in very high magnetic fields (up to 50–60 T, and above) using a variety of microwave and far-infrared sources [14–18]. It is worth to mention that high-field multiple-frequency (sometimes called tunable-frequency) ESR is a particular powerful technique to study frequency-field dependencies of magnetic excitations, providing important information on the nature of the ground state, magnetic structure, and peculiarities of magnetic interactions in numerous magnetic systems.

Here, we focus on ESR studies of copper pyrimidine dinitrate $[PM–Cu(NO_3)_2(H_2O)_2]_n$ (PM = pyrimidine), hereafter Cu–PM, an $S = 1/2$ antiferromagnetic chain system with alternating *g*-tensor and the DM interaction. This material can be regarded as one of the best realizations of the quantum sine-Gordon spin-chain model known to date. The remainder of this paper is organized as follows. In Sec. 2, an overview of magnetic properties of Cu–PM is given. In Sec. 3, an overview of instrumental procedure is given. In Sec. 4, we present ESR studies of magnetic excitations in Cu–PM in the 1D critical regime. The interpretation of the ESR excitation spectrum is done employing the effective sine-Gordon quantum-field-theory approach [3,9], allowing to identify a complete set of solutions of the sine-Gordon equation for $S = 1/2$ AF chains with a staggered transverse field (one soliton and three breathers). In Sec. 5 the evolution of ESR parameters in the perturbative spinon regime ($T \sim J$) is studied. In this phase, thermal fluctuations compete with short-range-order spin correlations, resulting in a pronounced change of ESR linewidth and shift, observed by us experimentally. These studies allow us to test a new theoretical concept proposed by Oshikawa and Affleck [19] for $S = 1/2$ AF chains with a staggered transverse field. In Sec. 6, we present results of ESR measurements of Cu–PM in magnetic fields up to 63 T, allowing us to study the transition from the 1D critical (with soliton-breather elementary excitations) to a spin-polarized state (with magnons forming the excitation spectrum). All the obtained experimental data are compared with results of existing theoretical concepts.

2. Structure and magnetic properties of copper pyrimidine dinitrate

$[PM–Cu(NO_3)_2(H_2O)_2]_n$ crystallizes in a monoclinic structure belonging to space group $C2/c$ with four formula units per unit cell [5]. The lattice constants obtained from the single-crystal x-ray diffraction are $a = 12.404$ Å, $b = 11.511$ Å, $c = 7.518$ Å, $\beta = 115.0^\circ$. Cu ions form chains (with a distance $d = 5.71$ Å between neighboring Cu^{2+} ions at 10 K) running parallel to the short ac diagonal (Fig. 1). The Cu ions are linked by the N–C–N moieties of pyrimidine, which constitute the intrachain magnetic exchange pathway. The interchain Cu–Cu distance is 6.84 Å. The Cu coordination sphere is a distorted octahedron, built from an almost square N–O–N–O equatorial plane and two oxygens in the axial positions. In this approximately tetragonal local symmetry, the local principal axis of each octahedron is tilted from the ac plane by $\pm 29.4^\circ$. Since this axis almost coincides with the principal axis of the *g*-tensor, the *g*-tensors for neighboring Cu ions are staggered.

In Fig. 2 experimental data for magnetic susceptibility for two different orientations of the applied magnetic field are shown. The data can be fit using the formula

$$\chi(T) = \chi_u(T) + \chi_s(T), \qquad (1)$$

where χ_u is the uniform susceptibility of the chain (which can be calculated using the Bethe ansatz [20]), while χ_s is

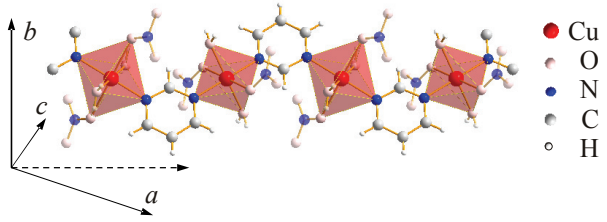

Fig. 1. (Color online) Schematic view of the crystal structure of Cu–PM, showing the alternation of octahedrons. The Cu chains are running parallel to the short ac diagonal (denoted by the dashed arrow).

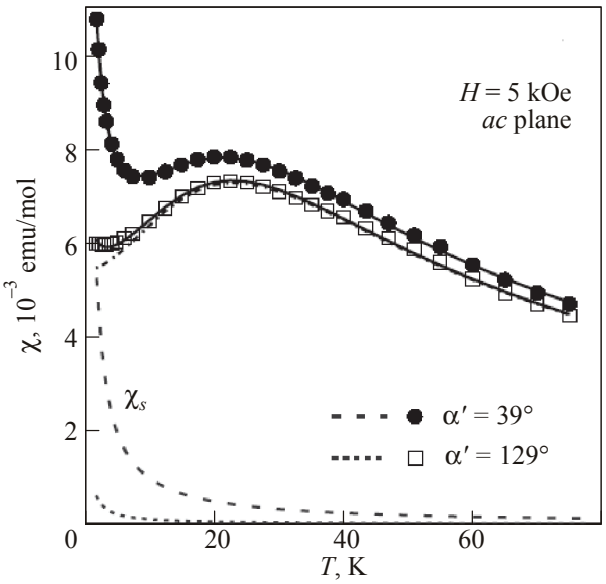

Fig. 2. Temperature dependence of magnetic susceptibility of Cu–PM for two orientations of magnetic field in the *ac* plane [5]. The staggered susceptibility is shown by dashed lines.

the staggered susceptibility. From this data, the exchange constant $J = 36 \pm 0.5$ K was extracted [5]. One can see that the magnetic susceptibility exhibits a strong anisotropy, which is an intrinsic property of $S = 1/2$ antiferromagnetic chains with alternating *g*-tensor or the Dzyaloshinskii–Moriya interaction.

As mentioned, the application of magnetic field induces a staggered magnetic moments, which opens an energy gap. For the first time, this gap was observed by means of specific heat and is shown in Fig. 3. The field-induced gap is maximal when magnetic field is applied along c'', which is the direction of maximal staggered magnetization.

High-field magnetization of Cu–PM with magnetic field applied along c'' direction at temperatures 1.6 and 4.2 K is shown in Fig. 4. A pronounced change of the magnetization derivative (shown in the inset) at $H_{\rm sat} = 48.5$ T indicates a transition into the spin polarized state. As revealed experimentally, the magnetization con-

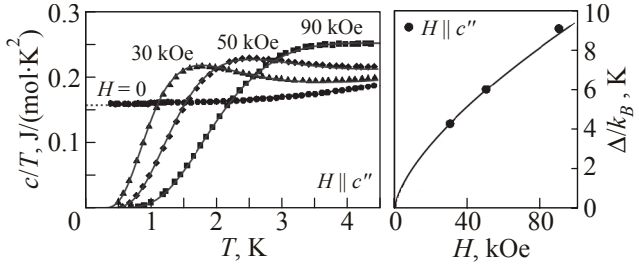

Fig. 3. Left: Temperature dependence of the specific heat of Cu–PM for different values of the applied magnetic field and $H \parallel c''$. Right: The magnetic field dependence of the field-induced gap as determined from specific heat measurements. The line is fit to the equation $\Delta \sim H^{2/3}$. The data are taken from Ref. 5.

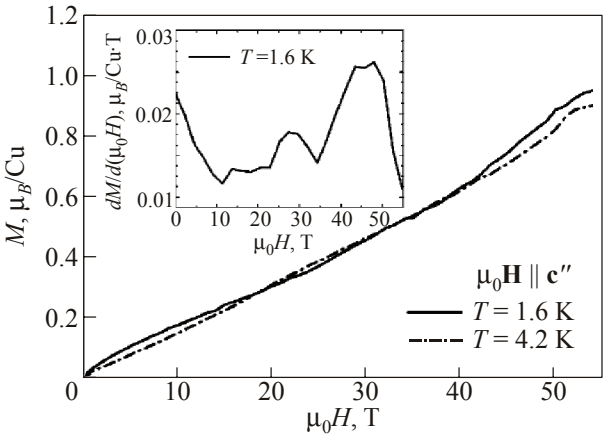

Fig. 4. Field dependence of the magnetization of Cu–PM with magnetic field applied along c'' direction for temperatures 1.6 and 4.2 K [21]. Inset: the field derivative of the magnetization is shown ($T = 1.6$ K).

tinues growing even above $H_{\rm sat}$ [21], revealing a significant role of the DM interaction in Cu–PM. Similar behavior appears to be a common feature of low-D magnets with DM interactions and was observed, e.g., in the natural mineral azurite [22].

3. Experimental procedure

ESR spectra were collected using two high-frequency spectrometers. ESR experiments up to 25 T were performed at the National High Magnetic Field Laboratory, Tallahassee, FL, USA [23]. Backward wave oscillators were employed as tunable sources of radiation, quasi-continuously covering the frequency range from 150 to 700 GHz. 25 T magnetic field was provided by a Bitter-type resistive magnet. Transmission-type probes in the Faraday and Voigt geometries equipped with oversized wave-guides were used.

ESR experiments in magnetic fields up to 63 T were performed at the Dresden High Magnetic Field Laboratory (Hochfeld-Magnetlabor Dresden, HLD, Helmholtz-Zentrum Dresden-Rossendorf, Germany) using a pulsed-field ESR spectrometer [18] equipped with VDI sources of millimeter- and sub-millimeter wave radiation sources (product of Virginia Diodes Inc.) and with a transmission-type probe in the Faraday configuration. A 8.5 MJ/70 T magnet was employed to generate pulsed magnetic fields with a pulse-field rise time of 35 ms and full-pulse durations of about 150 ms.

X-band ESR spectra were recorded using the Bruker ELEXSYS E580 spectrometer at a frequency 9.4 GHz.

High-quality single-crystals of Cu–PM with typical size of 3×3×0.5 mm were used. Magnetic field was applied along the c'' direction, which is characterized by the maximal value of the staggered magnetization for Cu–PM.

2,2-diphenyl-1-picrylhydrazyl (known as DPPH) was employed for the calibration of the magnetic field.

4. Excitations in 1D critical regime

If the temperature T is small compared to the energy gap Δ, but sufficiently high to prevent 3D long-range ordering, Cu–PM is in the 1D critical regime. In this phase, a Heisenberg $S = 1/2$ chain with exchange interaction J and DM interaction (or alternating g-tensor) in a field H can be mapped to a simple Heisenberg chain with a staggered transverse field $h \propto H$ [3,9,10], described by the effective spin Hamiltonian

$$\mathcal{H} = \sum_j [J\mathbf{S}_j \cdot \mathbf{S}_{j+1} + g\mu_B H S_j^z - h(-1)^j S_j^x]. \qquad (2)$$

As mentioned in Sec. 2, a field-induced gap in Cu–PM for the first time has been observed by means of specific heat [5]. This gap is formed by lowest-energy excitations, those frequency-field dependence can be studied directly, using high-field ESR techniques. In ESR experiments, several resonance modes were observed [24]. Typical ESR transmittance spectra obtained at frequencies of 429.3 and 245.3 GHz at temperature $T = 1.6$ K are shown in Fig. 5. It is worthwhile to mention that the low-temperature behavior of their integrated intensity, carefully checked at several temperatures down to 1.6 K, strongly suggests that the observed excitations correspond to the ground state transitions (details of the temperature evolution of the excitation spectrum in Cu–PM is given in Sec. 5).

The frequency-field diagram of magnetic excitations, obtained in magnetic fields up to 25 T at $T = 1.6$ K, is presented in Fig. 6 by filled symbols. The diagram can be analyzed

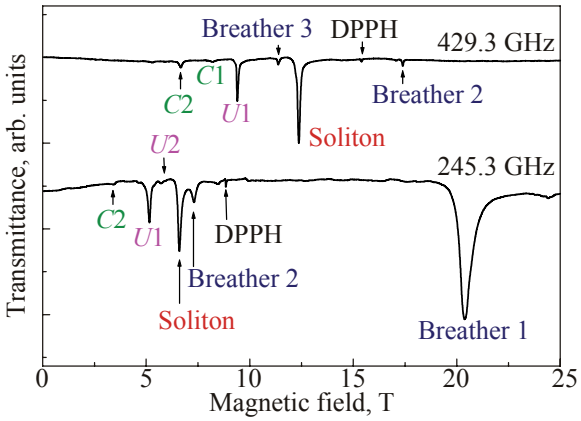

Fig. 5. (Color online) ESR spectra in Cu–PM, taken at frequencies 429.3 GHz (in the Faraday configuration) and 245.3 GHz (in the Voigt configuration) in magnetic fields up to 25 T, $T = 1.6$ K [24].

in the framework of the sine-Gordon quantum field theory [3,9]. The following expression [3] for the soliton gap, Δ_s, which is valid for fields up to $g\mu_B H \sim J$, can be used:

$$\Delta_s = \frac{J2\Gamma\left(\frac{\xi}{2}\right)v_F}{\sqrt{\pi}\Gamma\left(\frac{1+\xi}{2}\right)}\left[\frac{g\mu_B H}{Jv_F}\frac{\pi\Gamma\left(\frac{1}{1+\xi}\right)cA_x}{2\Gamma\left(\frac{\xi}{1+\xi}\right)}\right]^{\frac{1+\xi}{2}}. \qquad (3)$$

Here c is the proportionality coefficient connecting the uniform applied field H and the effective staggered field $h = cH$, the parameter $\xi = (2/(\pi R^2) - 1)^{-1}$, where R is the so-called compactification radius, and v_F has the meaning of the Fermi velocity. Both R and v_F are known exactly as functions of $\widetilde{H} = g\mu_B H / J$ from the solutions

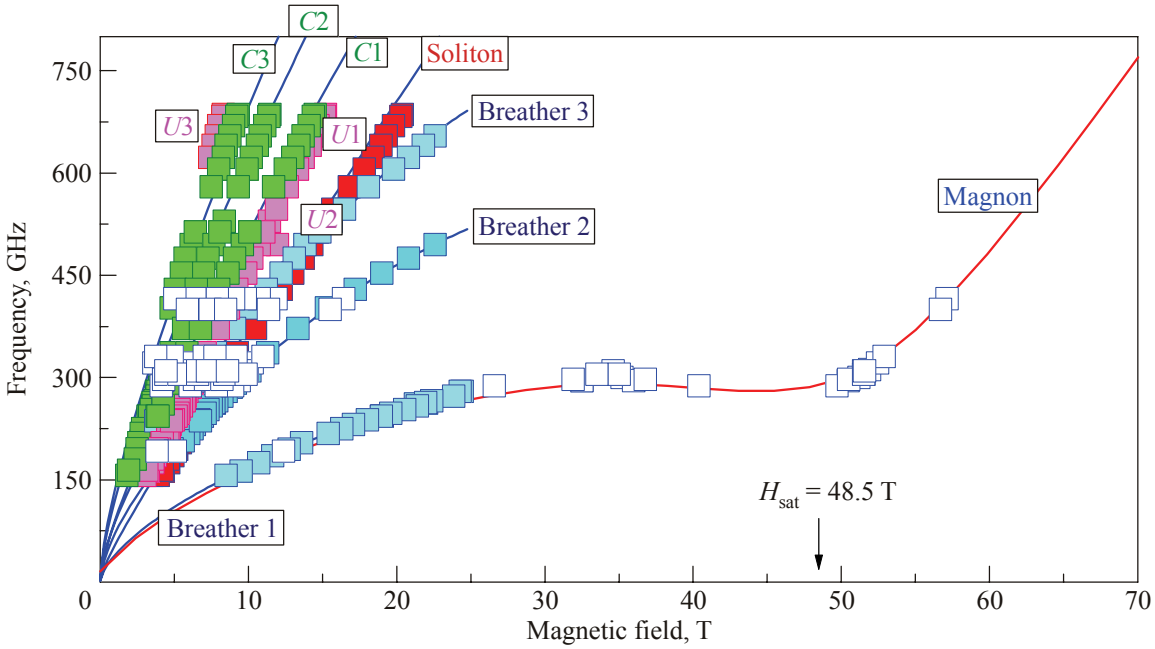

Fig. 6. (Color online) Frequency-field dependence of the detected ESR modes in Cu–PM [24,25]. Experimental data are denoted by symbols, and lines correspond to results obtained using the quantum-field sine-Gordon theory (blue lines) and DMRG calculations (red line). Note, that data denoted by open symbols are experimental results obtained using pulsed-field ESR.

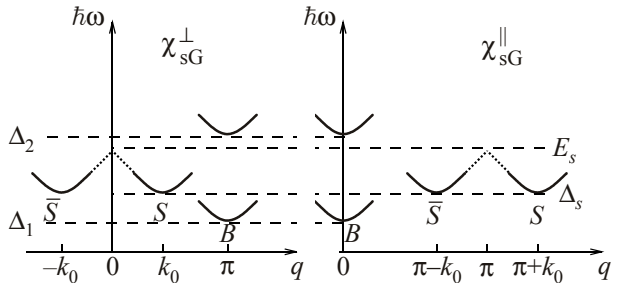

Fig. 7. A schematic view of the low-energy part of the excitation spectrum contributing to the transverse (left panel) and longitudinal (right panel) dynamic susceptibilities; $\bar{S}$ (S) denotes solitons and B labels breathers [24].

of the Bethe ansatz equations [3]. The amplitude A_x, which is also a function of $\widetilde{H}$, was recently computed numerically [12]. At a field H, there are $N = [1/\xi]$ breather branches B_n with $n = 1, \ldots N$. The breather gaps Δ_n are given by the formula

$$\Delta_n = 2\Delta_s \sin(n\pi\xi/2). \tag{4}$$

At $H = 0$ the first breather B_1 is degenerate with the soliton–antisoliton doublet S, $\bar{S}$. At finite H this degeneracy is lifted, so that the first breather, B_1, becomes the lowest excitation mode and gives the strongest contribution into the magnitude of the gap observed in specific heat experiments [5]. The sine-Gordon model predicts two more "heavier" breathers (B_2, B_3) to exist in the relevant frequency-field range.

It is widely accepted, that ESR probes the dynamical susceptibility $\chi(q, \omega)$ at the momentum $q = 0$. However, in the case of Cu–PM the alternation of the *g*-tensor and the DM interaction leads to a mixing of $q = 0$ and $q = \pi$ components, permitting the observation of ESR transitions at $q = \pi$. The energy structure of magnetic excitations for the sine-Gordon model contributing to the low-energy spin dynamics is sketched in Fig. 7. Single-particle contributions to the longitudinal susceptibility $\chi^{\parallel}_{sG}$ are determined by solitons located around incommensurate wave vectors $q = \pi \pm k_0$ and by breathers at $q = 0$. Here the incommensurate shift $k_0 = 2\pi m$ is determined by the total magnetization per spin *m*, exactly known as a function of the field; for small H one has $Jv_F k_0 \approx g\mu_B H$. In the transverse susceptibility $\chi^{\perp}_{sG}$ the dominating contribution comes from breathers at $q = \pi$ and solitons at $q = \pm k_0$. Thus, several breather resonances at the energies Δ_n, as well as a single soliton resonance at

$$E_s \simeq \sqrt{\Delta_s^2 + (Jv_F k_0)^2}, \tag{5}$$

are expected. Apart from single-particle resonances (see Fig. 7), there are various multiparticle continua contributing to the spectrum. Edges of those continua can be observed using ESR.

It is important to mention that in Eqs. (3)–(5) *the only* one free fitting parameter, coefficient *c*, is used. Setting $c = 0.08 \pm 0.002$, we were able to achieve an excellent fit to the lowest observed mode B_1, which is described by the first breather gap Δ_1. Using this value of *c*, the energies of other modes predicted by the sine-Gordon model were calculated; a reasonably good fit to the entire set of the experimental data was obtained. On the basis of the fit, the observed resonances were identified as denoted in Fig. 6. The interpretation of the soliton mode is supported by the analysis of the temperature dependence of the ESR spectra, which shows that the soliton mode continuously transforms into the $\omega = gH$ resonance when the temperature increases, in agreement with the theory [19]. The overall agreement between the sine-Gordon theory predictions and the experimentally obtained frequency-field dependence for those four single-particle resonances is very good. Our ESR results are consistent with experimental data obtained on $KCuGaF_6$ [8] and copper benzoate [26].

The identification of the other six high-frequency ESR modes is more challenging since the theory does not predict any single-particle contributions in the relevant frequency region. One may nevertheless speculate that the frequency-field diagram of modes $C1 - C3$ is very close to that of the edges of the soliton-breather continua SB_1, SB_2 and SB_3 (Fig. 5). The modes $U1 - U3$ can be related to chain-edge effects; this interpretation has been recently suggested in Refs. 27, 28. Noticeable, the presence of the additional modes have been revealed also in the $KCuGaF_6$ [8] and copper benzoate [29].

5. Electron spin resonance in 1D perturbative regime

If the temperature is high enough to suppress soliton-breather excitations, but sufficiently small compared to the characteristic energy of the exchange interaction J, the effect of alternating *g*-tensor and the Dzyaloshinskii–Moriya interaction can be regarded as a perturbation. In its absence, i.e., in an ideal $S = 1/2$ Heisenberg AFM chain, the resonance would occur exactly at the frequency $\hbar\omega = g\mu_B H$, having a zero linewidth in the low-temperature limit due to the conservation of the total S^z. In the Oshikawa–Affleck theory [19], the sole effect of the symmetry-breaking perturbation on the Green function is to produce the self-energy contribution Σ whose real and imaginary part determine the frequency shift and the linewidth, respectively. Other possible symmetry-breaking contributions arising, e.g., from the exchange anisotropy, can be distinguished by the characteristic dependence of the linewidth and the frequency shift on the magnetic field and the temperature [19]. Importantly, the theory allows a *precise* calculation of the ESR parameters and their dependence on temperature and magnetic field.

For the first time the significant changes in ESR spectra at low temperatures were observed in copper benzoate [30,31] (although the data were mistakenly explained in terms of the 3D ordering scenario). Later on, it was found

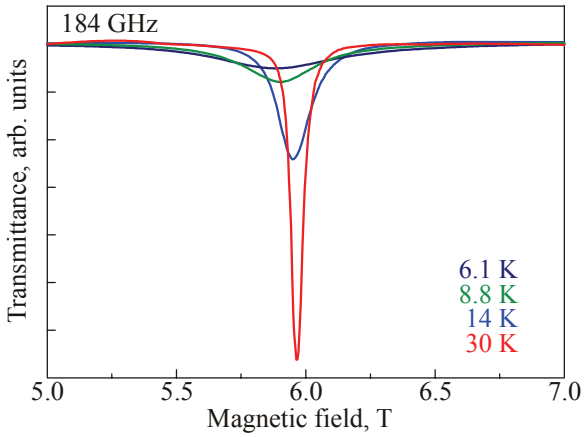

Fig. 8. (Color online) The ESR spectra of Cu–PM taken at a frequency of 184 GHz at four different temperatures [33].

[32] that terms $(H/T)^2$ and $(H/T)^3$ clearly dominate in the ESR linewidth and shift of the resonance field, respectively, being consistent with the Oshikawa–Affleck theory.

A detailed study of the temperature and field evolution of the ESR spectrum in Cu–PM in the 1D perturbative regime is reported in Ref. 33. Typical absorption spectra in Cu–PM at a frequency of 184 GHz at different temperatures are shown in Fig. 8. One can see that upon cooling the resonance becomes broader, while the absorption maximum shifts towards lower fields. Such a behavior is consistent with that observed earlier in copper benzoate [32] and $BaCu_2Ge_2O_7$ [34]. In our experiments the temperature dependence of the linewidth has been studied at three frequencies, 9.4, 93.1, and 184 GHz. The corresponding data are summarized in Fig. 9, together with results of the Oshikawa–Affleck theory. To fit the data, the following expression [19] has been used for the ESR linewidth ΔH:

$$\Delta H = \eta_0 + FzH\ \mathrm{Im}\,(G), \qquad (6)$$

where $z = \Gamma(1/4)/\Gamma(3/4)$ and $\Gamma(x)$ denotes the gamma function, and

$$G(H,T) = \Gamma\left(\frac{1}{4} - i\,\frac{g\mu_B H}{2\pi T}\right)/\Gamma\left(\frac{3}{4} - i\,\frac{g\mu_B H}{2\pi T}\right),$$

$$F(H,T) = c^2\sqrt{\pi/128}\,(J/T)\ln^{1/2}(\lambda J/T).$$

The constant λ in the leading log is to be viewed as a free phenomenological parameter compensating for the effects of subleading logarithmic terms. The overall correction η_0 takes into account that the ESR linewidth is in fact finite in the high-temperature ($T \gtrsim J$) regime. According to the theory, for $T \gg J$ the linewidth should become temperature-independent,

$$\Delta H \mapsto \eta_0 = \alpha + \beta(g\mu_B H/J)^2, \qquad (7)$$

finite α being caused by the DM interaction, and β containing contributions both from the DM interaction and from staggered g-tensor [19].

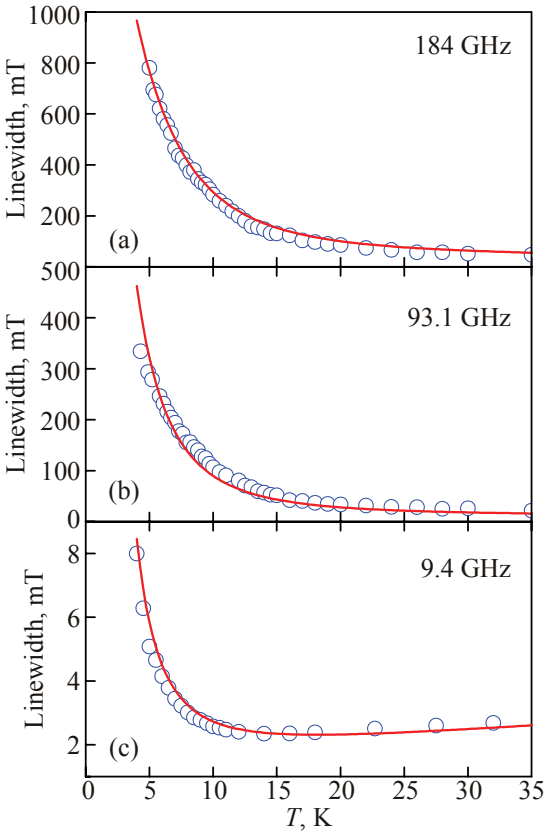

Fig. 9. (Color online) The temperature dependence of the ESR linewidth in Cu–PM at frequencies of 184 (a), 93.1 (b), and 9.4 (c) GHz [33]. Symbols denote the experimental results, and solid lines correspond to the best global fit using Eq. (6).

A very good fit to the entire set of the linewidth data is obtained, as shown in Fig. 9, with the following values of the parameters: $c = 0.083 \pm 0.001$, $\lambda = 2.0 \pm 0.05$, $\alpha = (1.5 \pm 0.2)$ mT, and $\beta = (830 \pm 25)$ mT. It should be mentioned that inclusion of log corrections turns out to be important: neglecting them makes it impossible to achieve a uniformly good fit for different frequencies. The obtained staggered field parameter c is in excellent agreement with

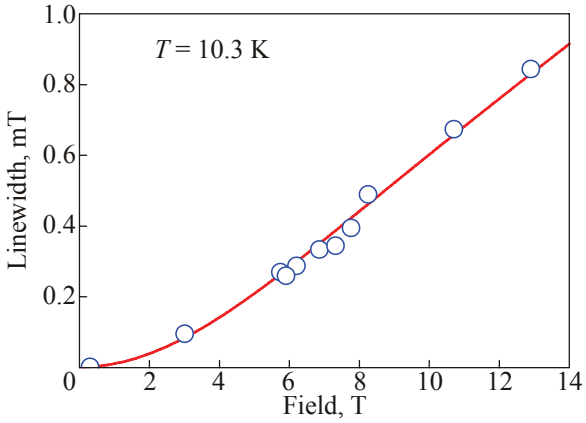

Fig. 10. (Color online) The field dependence of the ESR linewidth in Cu–PM at $T = 10.3$ K [33]. The solid line corresponds to Eq. (6) with the parameters obtained from the fit as described in the text.

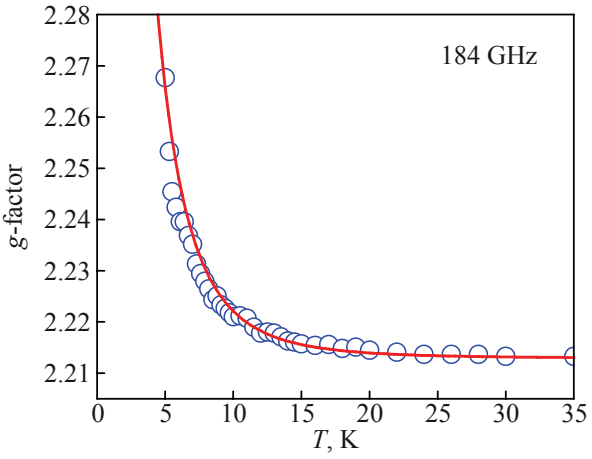

Fig. 11. (Color online) The temperature dependence of the effective g-factor in Cu–PM for a frequency of 184 GHz [33]. The solid line corresponds to Eq. (8) with the parameters obtained from the linewidth fit as described in the text.

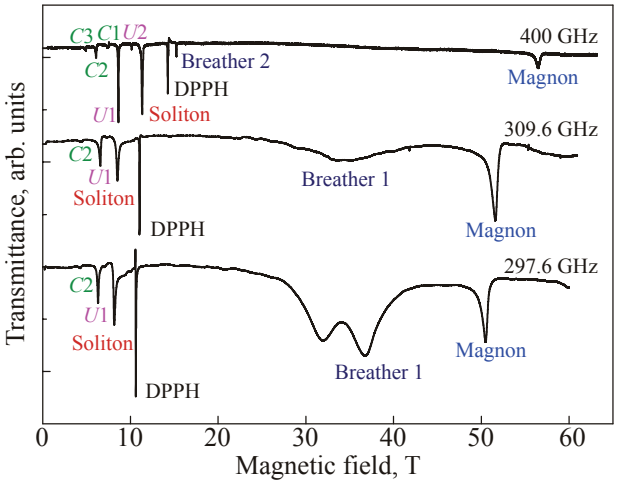

Fig. 12. (Color online) ESR spectra of Cu–PM, taken at frequencies of 297.6, 309.6, and 400 GHz at $T = 1.9$ K [25].

the value $c = 0.08 \pm 0.002$ found by us earlier from the analysis of the frequency-field dependence of ESR modes in Cu–PM in the soliton-breather regime [24]. The field dependence of the linewidth measured in fields up to 13 T at temperature of 10.3 K is shown in Fig. 10, together with the results of calculations using parameters obtained as described above. The data are in excellent agreement with the calculated values.

As seen in Fig. 9(c), at 9.4 GHz the temperature dependence of the linewidth contains a tiny (note the scale) contribution linearly growing in T. According to the theory [19,35], this can be caused by a small exchange anisotropy yielding the ESR linewidth contribution growing with the temperature.

Let us now discuss the behavior of g-factor. The experimental data for a frequency of 184 GHz are presented in Fig. 11, together with the theoretical curve described by the expression [19]

$$\Delta g = Fz(z - \mathrm{Re}\,(G)), \qquad (8)$$

where Δg is the dimensionless resonance frequency shift with respect to the g value at room temperature. The same parameter values as obtained from fitting the linewidth data has been used. An excellent agreement with the theory can be seen. For the chosen value of H the breather gap $E_g \approx 6$ K, which shows that the Oshikawa–Affleck theory actually works fairly well down to $T \sim E_g$.

6. Field-induced soliton–magnon crossover

As shown in Sec. 4, the sine-Gordon quantum field theory [3,9,10] applied for Cu–PM predicts that the elementary excitation spectrum is to be formed by solitons and their multiple bound states (breathers) with an energy gap $\Delta \propto H^{2/3}$ formed by the first breather mode [24,26]. The predictions of the sine-Gordon theory are limited to the range of small to moderate fields (up to $g\mu_B H \sim J$). Numerical simulations based on the density matrix renormalization group (DMRG) by Zhao *et al.* [36] have shown that when the field approaches the saturated phase, the energy gap is a nonmonotonous function of the field, having a minimum around the saturation field before the linear increase above the saturation. This result has been understood in analytical terms by Fouet *et al.* [37], who have shown, using field-theory arguments, that the gap around the saturation field in 1D spin systems scales as $h^{4/5}$. This exponent is larger than the exponent that controls the gap opening at low field, and for a small enough proportionality constant between the staggered field and the external field, this can lead to a local minimum of the gap around the saturation field. Such remarkable changes in the excitation spectrum in the vicinity of the saturation field ($H_{\mathrm{sat}} \approx 27$ T) have been identified experimentally first in copper benzoate [26]. The obtained data are in qualitative agreement with results of DMRG calculations [36].

The excitation spectrum of Cu–PM was studied in magnetic fields up to 63 T [25], using pulsed-field ESR facilities at the Dresden High Magnetic Field Laboratory [18]. In Fig. 12, typical pulsed-field ESR spectra taken in Cu–PM at 1.9 K and at frequencies of 297.6, 309.6, and 400 GHz are shown. Several very pronounced ESR modes are resolved. Data obtained in magnetic fields up to 25 T [24] and results of the pulsed-field ESR experiments are compiled in Fig. 6 using filled and open symbols, respectively. Apart from soliton and three breather modes, additional ESR modes were observed, including the ones labeled by $C1 - C3$ (which correspond to the edges of the soliton-breather continua) and the mode $U1$, which can be related to bound states due to chain-edge effects [27,28].

As mentioned, the spin gap at high fields ($H > J/g\mu_B$) can be calculated using DMRG calculations. The results of the DMRG calculations for the field-induced gap using the

microscopic model described by the Hamiltonian (Eq. (2)) with $L = 200$ lattice sites and $c = 0.083$ are shown in Fig. 6 by a blue solid line. These results were obtained by performing up to 10 DMRG sweeps and keeping up to $m = 500$ states, resulting in a discarded weight $\varepsilon \ll 10^{-10}$. It is worth to mention, that the DMRG results are in very good agreement with the prediction of the sine-Gordon theory in its limit of validity (low field). More importantly, the agreement between the DMRG results and the experimental results is excellent at all values of the field, in particular up to $H_{\rm sat}$ and above. Thus, the microscopic model of Eq. (2) provides a quantitative description of the spin-gap behavior in $S = 1/2$ sine-Gordon chains for all values of the field.

Let us comment now on the physical mechanism behind the nonmonotonic increase of the gap. In the absence of a staggered field, the system is gapless below saturation field, $H_{\rm sat}$. In the fully spin-polarized state above $H_{\rm sat}$ elementary excitations are magnons, and the gap opens linearly with $H - H_{\rm sat}$. The presence of a staggered field perpendicular to the external field opens a gap in the spectrum because it breaks the rotational symmetry around the field. Close to the saturation, the spins are almost polarized, and the system cannot develop a large transverse staggered magnetization. So the staggered field is less efficient to open a gap close to saturation than at low field. This is the basic mechanism behind the different scalings of the gap with c at low field ($\Delta \propto c^{2/3}$) and close to saturation ($\Delta \propto c^{4/5}$). For small enough c, this leads to a minimum of the gap around the saturation field. This explains the well-resolved dip in the frequency-field dependence of magnetic excitations in Cu–PM in the vicinity of $H_{\rm sat}$. Such a behavior appears to be a general feature of the high-field excitation spectrum of quantum $S = 1/2$ chain systems with alternating *g*-tensor or DM interactions.

7. Conclusion

In conclusion, our recent achievements on experimental studies of the spin dynamics in the copper pyrimidine dinitrate, an $S = 1/2$ antiferromagnetic chain material with alternating *g*-tensor and the Dzyaloshinskii–Moriya interaction, are presented. Employing ESR spectroscopy as a tool to probe magnetic excitations we show that in the 1D critical regime the excitation spectrum can be effectively described using the sine-Gordon quantum-field-theory model and is formed by solitons and their bound states, breathers. The first breather is found to be responsible for the field-induced gap observed earlier by means of specific heat. Using pulsed-field ESR, the gap behavior is investigated in magnetic fields up to saturation field, $H_{\rm sat} = 48.5$ T, and above, where the spectrum is formed by magnons. We show that a transition from the sine-Gordon region (with soliton-breather elementary excitations) to a spin-polarized state (with magnon excitations) in copper pyrimidine dinitrate is characterized by a minimum of the gap in the vicinity of $H_{\rm sat}$. Our description is fully confirmed by the quantitative agreement over the entire field range of experimental data with the DMRG calculations for $S = 1/2$ Heisenberg chain with a staggered transverse field. The temperature and field evolution of ESR parameters in the higher-temperature 1D perturbative regime is studied as well. The experimental data are compared with results of existing theoretical approaches, revealing an excellent agreement with the predictions.

Acknowledgment

This work was partly supported by the Deutsche Forschungsgemeinschaft and EuroMagNET (EU contract No. 228043). I would like to thank my collaborators, who participated in this project: A.K. Kolezhuk, J. Krzystek, R. Feyerherm, M. Ozerov, J. Wosnitza, E. Čižmár, S.R. Manmana, and F. Mila.

1. G. Müller, H. Thomas, H. Beck, and J.C. Bonner, *Phys. Rev. B* **24**, 1429 (1981).
2. M.B. Stone, D.H. Reich, C. Broholm, K. Lefmann, C. Rischel, C.P. Landee, and M.M. Turnbull, *Phys. Rev. Lett.* **91**, 037205 (2003).
3. I. Affleck and M. Oshikawa, *Phys. Rev. B* **60**, 1038 (1999); *ibid*. **62**, 9200 (2000).
4. D.C. Dender, P.R. Hammar, D.H. Reich, C. Broholm, and G. Aeppli, *Phys. Rev. Lett.* **79**, 1750 (1997); T. Asano, H. Nojiri, Y. Inagaki, J.P. Boucher, T. Sakon, Y. Ajiro, and M. Motokawa, *Phys. Rev. Lett.* **84**, 5880 (2000).
5. R. Feyerherm, S. Abens, D. Günther, T. Ishida, M. Meißner, M. Meschke, T. Nogami, and M. Steiner, *J. Phys.: Condens. Matter* **12**, 8495 (2000).
6. M. Kohgi, K. Iwasa, J.M. Mignot, B. Fak, P. Gegenwart, M. Lang, A. Ochiai, H. Aoki, and T. Suzuki, *Phys. Rev. Lett.* **86**, 2439 (2001).
7. M. Kenzelmann, Y. Chen, C. Broholm, D.H. Reich, and Y. Qiu, *Phys. Rev. Lett.* **93**, 017204 (2004).
8. I. Umegaki, H. Tanaka, T. Ono, H. Uekusa, and N. Nojiri, *Phys. Rev. B* **79**, 184401 (2009).
9. M. Oshikawa and I. Affleck, *Phys. Rev. Lett.* **79**, 2883 (1997).
10. F.H.L. Essler, *Phys. Rev. B* **59**, 14376 (1999).
11. F.H.L. Essler and A.M. Tsvelik, *Phys. Rev. B* **57**, 10592 (1998).
12. F.H.L. Essler, A. Furusaki, and T. Hikihara, *Phys. Rev. B* **68**, 064410 (2003).
13. K. Katsumata, *J. Phys.: Condens. Matter* **12**, R589 (2000).
14. H. Nojiri, Y. Shimamoto, N. Miura, M. Hase, K. Uchinokura, H. Kojima, I. Tanaka, and Y. Shibuya, *Phys. Rev. B* **57**, 10276 (1998).
15. S. Schmidt, B. Wolf, M. Sieling, S. Zvyagin, I. Kouroudis, and B. Lüthi, *Solid State Commun*. **108**, 509 (1998); M.

Sieling, U. Löw, B. Wolf, S. Schmidt, S. Zvyagin, and B. Lüthi, *Phys. Rev. B* **61**, 88 (2000).
16. M. Hagiwara, S. Kimura, H. Yashiro, T. Kashiwagi, H. Yamaguchi, and K. Kindo, *Appl. Magn. Res*. **36**, 269 (2009).
17. H. Ohta, S. Okubo, N. Souda, M. Tomoo, T. Sakurai, T. Yoshida, E. Ohmichi, N. Fujisawa, H. Tanaka, and R. Kato, *Appl. Magn. Res.* **35**, 399 (2009).
18. S.A. Zvyagin, M. Ozerov, E. Čižmár, D. Kamenskyi, S. Zherlistyn, T. Herrmannsdörfer, J. Wosnitza, R. Wünsch, and W. Seidel, *Rev. Sci. Instr.* **80**, 073102 (2009).
19. M. Oshikawa and I. Affleck, *Phys. Rev. Lett.* **82**, 5136 (1999); *Phys. Rev. B* **65**, 134410 (2002).
20. S. Eggert, I. Affleck, and M. Takahashi, *Phys. Rev. Lett.* **73**, 332 (1994).
21. A.U.B. Wolter, H. Rakoto, M. Costes, A. Honecker, W. Brenig, A. Klümper, H.-H. Klauss, F.J. Litterst, R. Feyerherm, D. Jérome, and S. Süllow, *Phys. Rev. B* **68**, 220406(R) (2003).
22. H. Kikuchi, Y. Fujii, M. Chiba, S. Mitsudo, T. Idehara, T. Tonegawa, K. Okamoto, T. Sakai, T. Kuwai, and H. Ohta, *Phys. Rev. Lett.* **94**, 227201 (2005).
23. S.A. Zvyagin, J. Krzystek, P.H.M. van Loosdrecht, G. Dhalenne, and A. Revcolevschi, *Physica* **B346**–**347**, 1 (2004).
24. S.A. Zvyagin, A.K. Kolezhuk, J. Krzystek, and R. Feyerherm, *Phys. Rev. Lett.* **93**, 027201 (2004); S.A. Zvyagin, J. Wosnitza, A.K. Kolezhuk, J. Krzystek, and R. Feyerherm, *J. Phys. Conf. Ser*. **51**, 39 (2006).
25. S.A. Zvyagin, E. Čižmár, M. Ozerov, J. Wosnitza, R. Feyerherm, S.R. Manmana, and F. Mila, *Phys. Rev. B* **83**, 060409(R) (2011).
26. H. Nojiri, Y. Ajiro, T. Asano, and J.-P. Boucher, *New J. Phys.* **8**, 218 (2006).
27. J. Lou, C. Chen, J. Zhao, X. Wang, T. Xiang, Z. Su, and L. Yu, *Phys. Rev. Lett.* **94**, 217207 (2005); J. Lou, C. Chen, and X. Wang, *Phys. Rev. B* **73**, 092407 (2006).
28. S.C. Furuya and M. Oshikawa, *arXiv:1112.1088v1*.
29. T. Asano, H. Nojiri, Y. Inagaki, T. Sakon, J.-P. Boucher, Y. Ajiro, and M. Motokawa, *Physica B* **329**–**333**, 1213 (2003).
30. M. Date, H. Yamazaki, M. Motokawa, and S. Tazawa, *Prog. Theor. Phys.* Suppl. **46**, 194 (1970).
31. K. Okuda, H. Hata, and M. Date, *J. Phys. Soc. Jpn.* **33**, 1574 (1972).
32. T. Asano, H. Nojiri, Y. Inagaki, J.P. Boucher, T. Sakon, Y. Ajiro, and M. Motokawa, *Phys. Rev. Lett.* **84**, 5880 (2000).
33. S.A. Zvyagin, A.K. Kolezhuk, J. Krzystek, and R. Feyerherm, *Phys. Rev. Lett.* **95**, 017207 (2005).
34. S. Bertaina, V.A. Pashchenko, A. Stepanov, T. Masuda, and K. Uchinokura, *Phys. Rev. Lett.* **92**, 057203 (2004).
35. A.A. Zvyagin, *Phys. Rev. B* **63**, 172409 (2001).
36. J.Z. Zhao, X.Q. Wang, T. Xiang, Z.B. Su, and L. Yu, *Phys. Rev. Lett.* **90**, 207204 (2003).
37. J.-B. Fouet, O. Tchernyshyov, and F. Mila, *Phys. Rev. B* **70**, 174427 (2004).